Radar Scattering Models for the Identification of Buried Low-Metal Content Landmines

Friedrich Roth[a], Piet van Genderen[a], Michel Verhaegen[b]
[a] International Research Centre for Telecommunications-Transmission and Radar
[b] Delft Center for Systems and Control
Delft University of Technology
Delft, The Netherlands

***Abstract*—Identification of buried antipersonnel landmines with ground penetrating radar (GPR) establishes a need for scattering models relating the measured scattered field to target characteristics such as size, material composition and burial depth. In this paper, we present generalizations of our previously published convolutional models for plane wave backscattering from a dielectric minelike target embedded in an unbounded host medium, which account for the ground surface, the GPR hardware and internal mine structure. Using 3D finite-difference time-domain (FDTD) and measured data examples, we illustrate the validity of the convolutional models and how they can be used to characterize buried targets. In particular, we show that it is possible to determine target size and depth with millimeter accuracy under laboratory conditions, both of which are valuable information for landmine identification.**

Keywords-ground penetrating radar (GPR); buried landmine identification; convolutional model.

I. INTRODUCTION

Future landmine detection systems will use combinations of different types of sensors to increase the detection and reduce the false alarm rate. When used in such a combination, GPR can help to reduce the number of false alarms by its capability to provide crucial target information, such as target size and depth of burial. To extract this information from measured GPR data, it is necessary to have practical models relating the target response to target characteristics. In this paper, we present generalizations of our previously published convolutional models for plane wave backscattering from a dielectric minelike target embedded in an unbounded host medium [1], [2], which account for the ground surface, the GPR hardware and internal mine structure. In doing so, we focus on circular disk-shaped targets, which are representative for a large class of landmines, e.g. *Type 72* and *PMA-3*. In section II, we start off by presenting a convolutional model for the GPR response of a target without internal structure. How this model can be used together with deconvolution to characterize a buried target is explained in section III and illustrated by examples based on 3D FDTD simulations and GPR data in sections IV and V, respectively. Finally, in section VI, we look at the effect of internal mine structure, specifically an air gap or a small metal part, and present an expression describing their contribution to the target impulse response.

This research was funded by the Dutch Technology Foundation STW.

II. SCATTERING FROM A CIRCULAR HOMOGENEOUS DIELECTRIC DISK BURIED IN THE GROUND

A. Target Impulse Response Approximation

A circular homogeneous dielectric disk differentiates the waveform of the incident wave. Its far-field axial impulse response can be approximated by

$$\mathrm{h_t}(t) = -\frac{v_\mathrm{t}^{eff} S_{xy} \Delta\varepsilon_r}{4\sqrt{\pi} c^2}\left(\dot{\delta}(t) - \Gamma\dot{\delta}\left(t - 2l/v_\mathrm{t}^{eff}\right)\right) \qquad (1)$$

[1], where S_{xy}, l and $\Delta\varepsilon_r$ are the disk's cross-section, height and relative permittivity contrast, v_t^{eff} is the effective velocity of the wave propagating through the disk, c is the vacuum speed of light, Γ is an attenuation factor, and $\dot{\delta}(t)$ denotes the 1st derivative of the delta function $\delta(t)$, i.e. a differentiation operator.

B. Convolutional Model for the Half-Space Problem

Equation (1) was originally derived from the volume integral representation of the backscattered field for the case that the disk is embedded in an unbounded host medium with the same properties as the ground [2]. In a recent derivation, we accounted for the presence of the ground surface by applying a far-field approximation of the half-space Green's tensor based on Banos' asymptotic expressions for the field due to a horizontal point electric dipole in the ground [3]. The derivation resulted in a convolutional model relating the backscattered field $\mathbf{e}^s$ at a height h above the ground to the field $\mathbf{e}^i$ incident on the disk located at a depth d:

$$\mathbf{e}^s(\boldsymbol{x},t) = \frac{T_{g\to a}\,\zeta(h,d)}{2\sqrt{\pi}(h+d)}\delta\left(t - \frac{h}{c} - \frac{d}{v}\right) \otimes \mathrm{h_t}(t) \otimes \mathbf{e}^i(\boldsymbol{x}_\mathrm{t},t)\ , \qquad (2)$$

where $v = c/\sqrt{\varepsilon_r}$ is the wave velocity in the ground, $T_{g\to a}$ is the normal incidence ground-to-air Fresnel transmission coefficient, and ζ is a coefficient accounting for the diffraction induced spreading at the ground surface and is defined as

$$\zeta(h,d) = \frac{h+d}{h\sqrt{\varepsilon_r} + d} \quad . \tag{3}$$

C. Convolutional GPR Signal Model

For application to GPR, the radar hardware needs to be incorporated into the convolutional model of (2). We model the transmitting antenna as a point source positioned at a height h_{TX} above the ground from which the radiated field is assumed to propagate spherically with a 1/*r* amplitude decay while maintaining its waveform. The receiver chain including the receiving antenna is modeled as a point receiver positioned below the transmitting antenna at a height h_{RX} and is characterized by an impulse response relating the scattered field at the receiving antenna, $\mathbf{e}^s$ in (2), to the measured target response signal $\mathrm{s}(t)$. Based on these hardware models, we may write

$$\mathrm{s}(\boldsymbol{x}_{\mathrm{RX}}, t) = \frac{T_{g\to a}\zeta(h_{\mathrm{RX}}, d)T_{a\to g}}{2\sqrt{\pi}(h_{\mathrm{RX}}+d)(h_{\mathrm{TX}}+d)} \otimes \mathrm{h}_{\mathrm{t}}(t) \otimes \mathrm{w}\left(t - \frac{h_{\mathrm{RX}}+h_{\mathrm{TX}}}{c} - \frac{2d}{v}\right), \tag{4}$$

where $T_{a\to g}$ is the normal incidence air-to-ground Fresnel transmission coefficient and $\mathrm{w}(t)$ is the effective radiated waveform defined as the convolution of the actual radiated waveform and the impulse response of the receiver chain.

III. Deconvolution and Target Identification

To identify a target, we use subset selection deconvolution [4] to fit an impulse response of the form

$$\mathrm{h}(t) = \mathrm{h}_1\dot{\delta}(t-\tau_1) - \mathrm{h}_2\dot{\delta}(t-\tau_2) \tag{5}$$

to the target response. The resulting impulse response can be related to target characteristics by means of (1)-(4). Note from (1) that target size and target contrast are inherently unresolved, i.e. an increase in target cross-section cannot be distinguished from an increase in target contrast. Consequently, it is only possible to infer possible combinations of target characteristics. In the examples that follow, we chose to estimate the cross-section S_{xy} and the height *l* from the impulse response coefficient h_1 and the impulse response length $\tau_2 - \tau_1$, respectively, by assuming a contrast $\Delta\varepsilon_r$ and an effective velocity v_{t}^{eff} that are characteristic of the type of target to be identified.

IV. 3D FDTD Simulation Results

We simulated the axial responses of three buried circular dielectric disks having a relative permittivity of 2.8, which is representative for the explosive TNT, a radius between 3 and 7.5 cm, and a height of either 4 or 6 cm. The disks, referred to as *TNT Disk 1* through *3*, were considered at depths of 2.5 and 10 cm in a ground with a relative permittivity of 4. As incident field we used a linearly polarized plane wave whose time dependency is a Ricker wavelet with a peak amplitude frequency of 1.5 GHz.

From the simulated responses we deconvolved the incident field at the disk location, $\mathbf{e}^i(\boldsymbol{x}_{\mathrm{t}}, t)$ in (2). Fig. 1 gives an example of the generally good data fit between the simulated responses and the responses estimated by deconvolution, demonstrating that the axial responses of the disks are well modeled by an impulse response as in (5) consisting of two differential operators. Figs. 2 and 3 illustrate the relationship between the impulse response parameters obtained by deconvolution and disk size. We see that there is indeed a linear relationship between the coefficient h_1 and the cross-section S_{xy}, and between the impulse response length $\tau_2 - \tau_1$ and the disk height *l*, as predicted by (1). By fitting a straight line to the data points in Fig. 3, we find $v_{\mathrm{t}}^{eff} \approx 16.6$ cm/ns, which is slightly lower than $c/\sqrt{2.8} \approx 17.9$ cm/ns. Table I lists the results of inverting the impulse responses for disk radius and height. The good agreement between the estimated and the true disk dimensions (shown in parentheses) demonstrates that (1)-(3) accurately describe the scattering from a buried dielectric disk. Furthermore, the inversion results demonstrate that in principle it is possible to estimate disk radius and height with millimeter accuracy given that the observation height and the target depth are known. This, however, is no limitation because, in the case of measured GPR data, the observation height and the target depth can be determined from the arrival time of the ground reflection and that of the target response, as will be shown in the following section.

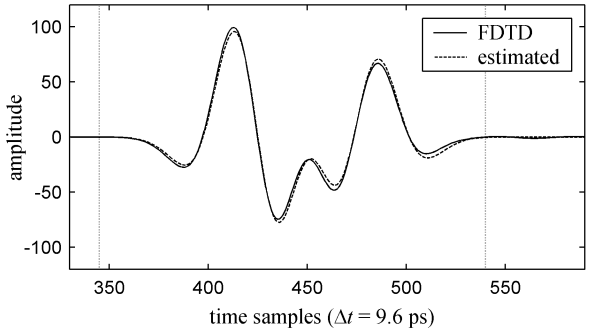

Figure 1. Data fit between the simulated and the estimated (deconvolution) response of *TNT Disk 1* (*d* = 2.5 cm & *h* = 30 cm).

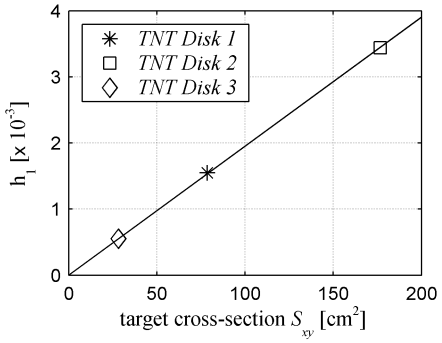

Figure 2. Deconvolution results for the *TNT Disks* (*d* = 2.5 cm & *h* = 30 cm): h_1 versus S_{xy}.
The straight line represents a least squares fit to the data points.

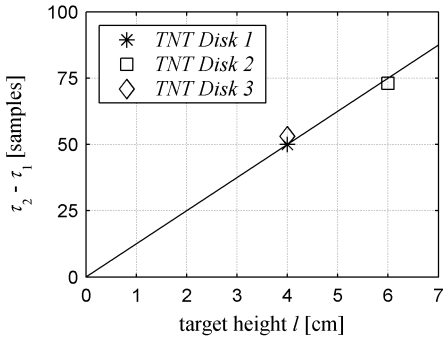

Figure 3. Deconvolution results for the *TNT Disks* (d = 2.5 cm & h = 30 cm): $\tau_2 - \tau_1$ versus l.
The straight line represents a least squares fit to the data points.

TABLE I. INVERSION RESULTS FOR THE TNT DISKS.

Target Name	**Target Depth**	**Observation Height**	**Inversion for Target Size***	
	d [cm]	h [cm]	target radius [cm]	target height l [cm]
TNT Disk 1	2.5	30.0	5.1 (5.0)	4.0 (4.0)
	10.0	30.0	5.2 (5.0)	4.0 (4.0)
TNT Disk 2	2.5	30.0	7.6 (7.5)	5.8 (6.0)
	10.0	30.0	7.7 (7.5)	5.8 (6.0)
TNT Disk 3	2.5	30.0	3.1 (3.0)	4.2 (4.0)
	10.0	30.0	3.1 (3.0)	4.2 (4.0)

* Based on $\Delta\varepsilon_r = 2.8 - 4 = -1.2$ and $v_t^{eff} = 16.6$ cm/ns .
The values included in parentheses are the true values.

V. EXPERIMENTAL RESULTS

For experimental verification, we used a laboratory video impulse radar to acquire B-scans over four buried circular disks made of Expandable Polystyrene (EPS), which has a relative permittivity of approximately 1. The radar uses the quasi-monostatic antenna system presented in [5], which is fed by a 0.8 ns pulse generator. The disks, referred to as *EPS Disk 1* through *4*, have a radius between 4 and 6.25 cm, and a height of either 3.8 or 4.8 cm. They were buried around 5 cm deep in dry sand having a relative permittivity of 2.6. Data were acquired for two receiving antenna heights, 15 and 20 cm. For all data, the vertical offset $h_{TX} - h_{RX}$ between the transmitting and the receiving antenna was 30.5 cm. Preprocessing was applied to reduce noise and to isolate the target responses from the direct wave and the ground reflection. The latter was achieved by a two-iteration weighted moving average background subtraction algorithm, which first finds the anomalies in the data and then suppresses them in the estimation of the background to be subtracted.

For each disk, the effective radiated waveform $w(t)$, estimated from a set of metal sheet reflection measurements with varying antenna heights, was deconvolved from the preprocessed A-scan at the apex of the target response hyperbola. Despite the presence of clutter due to disturbance of the sand, the data fit between the measured responses and the responses estimated by deconvolution was generally good, an example of which is shown in Fig. 4. Table II summarizes the results of inverting the impulse responses for disk radius and height. The listed receiving antenna heights and target depths, which are required for the size estimation, were determined from the arrival time of the ground reflection and that of the target response, i.e. τ_1. As for the simulated disks, we observe good agreement between the estimated and the true values (shown in parentheses).

VI. SCATTERING FROM A MINELIKE TARGET WITH INTERNAL STRUCTURE

To study the effect of internal mine structure, we also acquired B-scans over three buried circular Teflon disks, all having a radius of 5 cm and a height of 4 cm but differing internally: the first is solid, the second contains a thin circular air gap (50.3 cm^2 × 1 cm), and the third has a small cylindrical metal insert (2.7 cm^3). From a comparison of the measured responses, shown in Fig. 5, we found that the target response is determined by the presence of the air gap and to a much lesser extent by the metal insert. The same observation was made from repeating the FDTD simulation for *TNT disk 1*: first with a thin circular air gap (50.3 cm^2 × 1 cm) and second with a cubical metal inclusion (1 cm^3). The responses that resulted from these simulations are shown in Fig. 6.

The target impulse response model of (1) can be generalized to account for internal structure by introducing

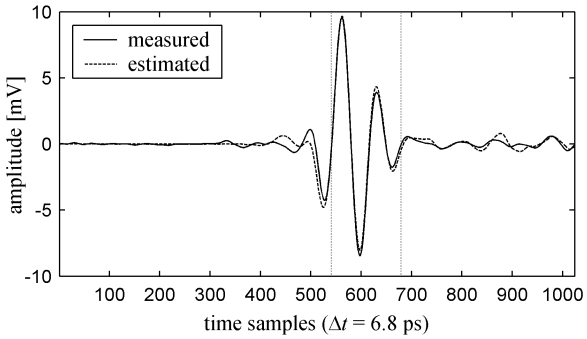

Figure 4. Data fit between the measured and the estimated (deconvolution) response of *EPS disk 1* ($d \approx 5$ cm & $h_{RX} \approx 15$ cm).

TABLE II. INVERSION RESULTS FOR THE EPS DISKS.

Target Name	**Target Depth Estimation**	**Antenna Height Estimation**	**Inversion for Target Size***	
	d [cm]	h_{RX} [cm]	target radius [cm]	target height l [cm]
EPS Disk 1	5.0 (4.9)	15.2 (15.1)	5.0 (5.0)	3.8 (3.8)
	5.0 (4.9)	20.1 (20.1)	4.9 (5.0)	3.7 (3.8)
EPS Disk 2	5.0 (4.9)	15.0 (15.1)	5.2 (5.0)	4.6 (4.8)
	5.0 (4.9)	19.9 (20.1)	5.1 (5.0)	4.3 (4.8)
EPS Disk 3	5.2 (5.3)	15.3 (14.7)	4.3 (4.0)	4.2 (3.8)
	5.2 (5.3)	20.1 (19.7)	4.2 (4.0)	4.2 (3.8)
EPS Disk 4	5.5 (5.4)	15.0 (14.6)	6.5 (6.25)	4.5 (4.8)
	5.5 (5.4)	19.7 (19.6)	6.5 (6.25)	4.6 (4.8)

* Based on $\Delta\varepsilon_r = 1 - 2.6 = -1.6$ and $v_t^{eff} = 28.5$ cm/ns (estimated from FDTD simulations).
The values included in parentheses are the true values.

appropriate contrast functions for the air gap and the metal inclusion in the volume integral equation from which (1) was derived. Using contrast functions that follow from the Rayleigh scattering approximation for small dielectric and PEC spheres [6], we find

$$\mathrm{h_t}\left(t\right) = \mathrm{h_t^{homog}}\left(t\right) - \frac{1}{2\sqrt{\pi}c^2}\xi\, V\, \ddot{\delta}\left(t - 2a/v_t^{eff}\right)\ , \qquad (6)$$

where $\mathrm{h_t^{homog}}$ is the impulse response of the dielectric disk if it were homogeneous, i.e. that given by (1), V is the volume of the gap/inclusion, $\ddot{\delta}(t)$ denotes the 2nd derivative of the delta function, a is the vertical position of the gap/inclusion from the top of the disk, and ξ is defined as

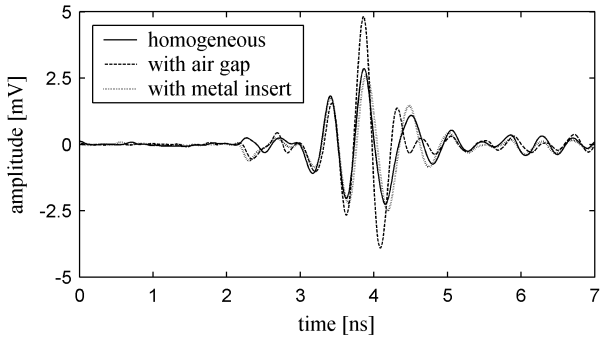

Figure 5. Comparison of the measured responses of the buried Teflon disks ($d \approx 5$ cm & $h_{RX} \approx 15$ cm).

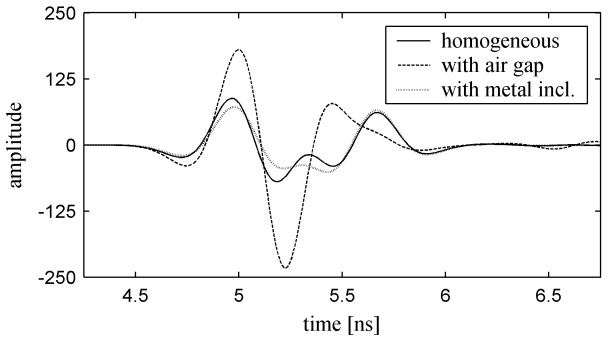

Figure 6. Simulated response of *TNT Disk 1* with and without internal structure (d = 10 cm & h = 30 cm).

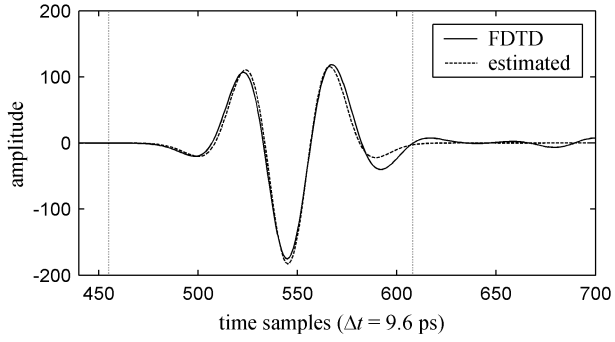

Figure 7. Data fit for the air gap response.

$$\xi = \begin{cases} \left(1-\varepsilon_r\right)\dfrac{3\varepsilon_r}{\left(1-\varepsilon_r\right)+3\varepsilon_r} - \Delta\varepsilon_r & \text{for a thin air gap} \\ \dfrac{9}{2}\varepsilon_r - \Delta\varepsilon_r & \text{for a small metal inclusion.} \end{cases} \qquad (7)$$

According to (6), the air gap and the metal inclusion differentiate the incident waveform twice. As a first check of (6) and (7), we looked at the responses of the air gap and the metal inclusion in *TNT Disk 1* separately by simply subtracting the homogenous disk response from the non-homogeneous disk responses, and fitted them with the 2nd derivative of the incident Ricker wavelet (see section IV). Fig. 7 shows the good data fit obtained for the air gap response. The data fit for the metal inclusion was equally good. In addition, from the magnitude of the responses we estimated volume using (6) and (7) in (2), giving 43.6 cm^3 for the air gap and 1.14 cm^3 for the metal inclusion, which are in good agreement with their true volumes (error < 15%).

VII. Conclusions

We have developed a convolutional model for the response of a buried minelike target as measured by GPR. The presented data examples demonstrate that the model adequately describes

- the target impulse response and its relation to target size and contrast
- the contribution of a thin air gap or a small metal part to the target impulse response
- the dependency of the target response magnitude on antenna height and target depth
- the GPR hardware (antennas, receiver chain).

The model can be used together with subset selection deconvolution to characterize a buried target based on a single A-scan, viz. the A-scan at the apex of the target response hyperbola. An interesting application is to determine target size and burial depth, which was found to be possible with millimeter accuracy under laboratory conditions.

References

[1] F. Roth, P. van Genderen, and M. Verhaegen, "Processing and analysis of polarimetric ground penetrating radar landmine signatures", in *Proc. of the 2nd Int. Workshop on Advanced Ground Penetrating Radar*, Delft, The Netherlands, 2003, pp. 70-75.

[2] F. Roth, P. van Genderen, and M. Verhaegen, "Radar response approximations for buried plastic landmines", in *Conf. Proc. SPIE*, vol. 4758, 9th International Conference on Ground Penetrating Radar, Santa Barbara, CA, 2002, pp. 234-239.

[3] A. Banos Jr., *Dipole Radiation in the Presence of a Conducting Half-Space*, Pergamon Press, 1966, ch. 5.

[4] F. van der Lijn, F. Roth, and M. Verhaegen, "Estimating the Impulse Response of Buried Objects from Ground Penetrating Radar Signals", *Conf. Proc. SPIE*, vol. 5089, Detection and Remediation Technologies for Mines and Minelike Targets VIII, Orlando, FL, 2003, pp. 387-394.

[5] A. G. Yarovoy, A. D. Schukin, I. V. Kaploun, and L. P. Ligthart, "Antenna system for UWB GPR for landmine detection", in *Conf. Proc. SPIE*, vol. 4394, Detection and Remediation Technologies for Mines and Minelike Targets VI, Orlando, FL, 2001, pp. 692-699.

[6] J. A. Kong, *Electromagnetic Wave Theory*, New York: John Wiley & Sons, 1986, pp. 482-485.